

Article



Hyperspectral Raman Imaging Using a Spatial Heterodyne Raman Spectrometer with a Microlens Array

Applied Spectroscopy 2020, Vol. 74(8) 921–931 © The Author(s) 2020 Article reuse guidelines: sagepub.com/journals-permissions DOI: 10.1177/0003702820906222 journals.sagepub.com/home/asp

\$SAGE

Ashley Allen , Abigail Waldron, Joshua M. Ottaway, J. Chance Carter , and S. Michael Angel

Abstract

A new hyperspectral Raman imaging technique is described using a spatial heterodyne Raman spectrometer (SHRS) and a microlens array (MLA). The new technique enables the simultaneous acquisition of Raman spectra over a wide spectral range at spatially isolated locations within two spatial dimensions (x, y) using a single exposure on a charge-coupled device (CCD) or other detector types such as a complementary metal-oxide semiconductor (CMOS) detector. In the SHRS system described here, a 4 × 4 mm MLA with 1600, 100 µm diameter lenslets is used to image the sample, with each lenslet illuminating a different region of the SHRS diffraction gratings and forming independent fringe images on the CCD. The fringe images from each lenslet contain the fully encoded Raman spectrum of the region of the sample "seen" by the lenslet. Since the SHRS requires no moving parts, all fringe images can be measured simultaneously with a single detector exposure, and in principle using a single laser shot, in the case of a pulsed laser. In this proof of concept paper, hyperspectral Raman spectra of a wide variety of heterogeneous samples are used to characterize the technique in terms of spatial and spectral resolution tradeoffs. It is shown that the spatial resolution is a function of the diameter of the MLA lenslets, while the number of spatial elements that can be resolved is equal to the number of MLA lenslets that can be imaged onto the SHRS detector. The spectral resolution depends on the spatial resolution desired, and the number of grooves illuminated on both diffraction gratings by each lenslet, or combination of lenslets in cases where they are grouped.

Keywords

Spatial heterodyne spectrometer, SHS, spatial heterodyne Raman spectrometer, SHRS, Raman, Raman imaging, microlens array, hyperspectral Raman imaging

Date received: 27 November 2019; accepted: 29 December 2019

Introduction

The spatial heterodyne Raman spectrometer (SHRS) is a fixed grating, Fourier transform interferometer with high light throughput, a wide field of view (FOV), and high spectral resolution. Unlike conventional, dispersive grating-based spectrometers, the resolving power of the SHRS is not strongly dependent upon entrance aperture size. The SHRS also has no moving parts, and SHS emission spectrometers have been built using monolithic optical techniques, which makes the system robust and tolerant of vibrations. The large acceptance angle of the SHRS makes it amenable to applications involving the collection of light from diffuse sources, or for remote Raman at intermediate ranges² where image jitter can affect the reproducibility when using a slit-based spectrometer. Applications such as remote Raman, transmission Raman, micro-Raman,

fiber coupled Raman, spatially offset Raman, and Raman imaging may benefit from the larger viewing area of the SHRS. This paper describes an innovative way to perform two-dimensional (2D) Raman chemical imaging using the SHRS, which takes advantage of the large viewing area of the SHS.

Raman imaging is useful to characterize heterogeneous materials by measuring chemical properties in multiple spatial dimensions.⁴ A Raman image can be 2D, where the

Department of Chemistry and Biochemistry, University of South Carolina, Columbia, USA

Corresponding author:

S. Michael Angel, University of South Carolina, 631 Sumter Street, Columbia, SC 29212, USA.
Email: smangel0@mailbox.sc.edu

intensity of a single Raman band is mapped across the heterogenous sample, or hyperspectral, where multiple Raman band intensities are acquired for each spatial point on the sample. Early Raman microprobes were scanning instruments, where the laser mapped the sample surface to generate the hypercube of data, either point-by-point or by line scanning the laser across the sample. For point-by-point scanning, the laser is focused to a small spot and the sample is raster scanned through the laser beam, collecting the entire Raman spectrum at each point.⁶ In line scanning, the laser is focused to a thin line, using cylindrical optics. The illumination line on the sample is parallel to the entrance slit of a dispersive spectrometer so that a Raman spectrum is acquired on each row of a 2D array detector. Wide field Raman imaging measures all points on the sample simultaneously using an expanded laser spot, while a single Raman band is measured using a tunable filter to acquire a 2D Raman image. The hyperspectral image is built up by measuring Raman images as the filter is tuned to different wavelengths corresponding to Raman bands. Various types of filters have been used in this method, including dielectric filters, acousto optic, and liquid crystal tunable filters.8-16 Fiber optic arrays have been used for hyperspectral Raman imaging, where spatial and spectral information were simultaneously acquired. However, the number of spatial points demonstrated using a fiber array is low and the fiber fill factor is also low. 17

Here, we describe a new hyperspectral Raman imaging technique using a microlens array (MLA) in a confocal imaging arrangement with an SHRS. The MLA is an array of microlenses, with diameters ranging from 10 µm to 2 mm, where each views a different spot on the sample. The use of MLAs for confocal microscopy has been described previously; Dwight and Tkaczyk reported fluorescence microscopy using an MLA with a prism to collect fluorescence data with \sim 20 nm spectral resolution. ¹⁸ This technique has not previously been applied to Raman. The MLA-SHRS instrument described in this paper allows the measurement of a hyperspectral Raman image, covering the entire Raman fingerprint range (e.g., \sim 2500 cm⁻¹) in a single measurement. In this proof of concept paper, approximately 550 spatially isolated Fizeau fringe patterns are simultaneously imaged; our data indicate that many thousands of points (e.g., \sim 10 000) can be simultaneously imaged while maintaining a large spectral range, in an optimized instrument.

Experimental

Illumination

The sample was excited by a continuous wave (CW) 532 nm neodymium-doped yttrium aluminum garnet (Nd:YAG) laser (OptoEngine, MLL-FN-532-300mW) in an epi-illumination backscatter geometry. The laser beam diameter was 2.2 mm. The laser was directed to the

sample on the axis of the SHRS spectrometer, using a 25 mm diameter, 550 nm long-pass dichroic mirror (ThorLabs, DMLP550), and was focused on the sample by the MLA (Suss MicroOptics, part no. 19-00055), with each lenslet focusing the laser to a separate small spot, with an airy disk of \sim 20 μ m, to give an array of 484 laser spots on the sample. The laser power focused by each separate lenslet was \sim 300 μ W at the sample. The sample was located at the focal point of the f/16 MLA, a distance of 1.5 mm. The fused silica MLA is 4×4 mm overall size with 1600, 100 μm diameter circular lenslets, packed in a square grid, with a fill factor close to 80%. The MLA has chromium apertures that block light between the lenslets to prevent crosstalk, and it is antireflection coated at 780 nm. The flat surface was turned opposite the sample, in the direction of the spectrometer.

Light Collection

Raman scattered light from the sample was collected by the MLA and collimated, each lenslet having a unique spatially isolated FOV on the sample from the others, producing its own separate collimated beam. A relay lens (Nikon AF NIKKOR 80–200 mm f/4.5–5.6) was used to image the back surface of the MLA onto the SHRS gratings. The distance used depended on the desired magnification, $4\times$, $8\times$, or $10\times$, of the MLA at the SHRS gratings. The magnification was used to change the number of lenslets measured and the resolving power for single lenslets. A 4 mm diameter spatial filter, located at the focal point of the relay lens, minimized crosstalk between lenslets, as described by Tiziani et al. $^{19.20}$

Spatial Heterodyne Spectrometer

The SHRS, similar to ones described previously, is equipped with a 25 mm N-BK7 non-polarizing 50:50 cube beamsplitter (ThorLabs, BS013) and a pair of 300 lp/mm gratings, blazed at 500 nm (Edmund Optics, #64-403).^{21,22} An iris at the input aperture limits the size of the illuminated area on the gratings to \sim 14 mm. The SHRS was equipped with two 532 nm long-pass filters (Semrock RazorEdge, LP03-532RE-25), a 550 nm long-pass filter (ThorLabs, FEL0550), and a 581 nm short-pass filter (Knight Optical, 581FDS25) to remove strong laser scatter and to limit the total spectral range (bandpass) allowed into the spectrometer. A fused silica 105 mm focal length, f/4.5 lens (Coastal Optical Systems, Inc., UV-MICRO-APO 111032) imaged the grating faces to produce the fringe image with 1.17× magnification onto a thermoelectrically cooled, back-illuminated, UV-enhanced charge-coupled device (CCD) detector with 2048×512 , 13.5 µm pixels (Princeton Instruments, PIXIS-2048 2KBUV). A spatial filter placed one focal length behind the imaging lens was used to block higher grating orders. Images were acquired in Lightfield 4.10 software with 100 kHz ADC gain high and in the low noise setting.

The CCD was cooled to $-70\,^{\circ}$ C. For the Raman image in Fig. 8, a CMOS detector with 5544 \times 3694, 2.4 μ m pixels was used (QHYCCD, QHY183M).

Spectral Calculations, Fast Fourier Transform

All spectral calculations were done using Matlab (The MathWorks, v.R2016a). To obtain Raman spectra from the fringe images, a region of interest is selected, and the rows are summed, in the vertical direction, to give an interferogram superimposed on a background signal, and the background is removed by subtracting a fitted polynomial curve. The corrected interferogram is then Fourier transformed using the Matlab FFT function, to reveal the Raman spectrum, plotted as magnitude versus wavenumber. For 2D SHRS measurements, one grating was slightly tilted from the vertical to produce a wavenumber dependent fringe rotation that reduces the ambiguity of bands above and below the Littrow wavenumber.

Sample Preparation

Several bilayer mixed sample pellets were prepared using a 13 mm pellet die (Carver, catalog #3619). Samples were prepared with the intention of keeping the constituents spatially separated so that different samples were viewed by different lenslets of the MLA. The samples included a diamond (Wards Science, kit #458200) pressed into a potassium perchlorate (Alfa Aesar #11630, 99% anhydrous) pellet, a sodium sulfate (Sigma Aldrich, 239313)/potassium perchlorate pellet, a sodium nitrate (Sigma Aldrich, 347663)/potassium perchlorate pellet, and an acetaminophen (Sigma-Aldrich, A7085)/ ammonium nitrate (Aldrich, 256064) pellet.

Results and Discussion

The SHRS is a dispersive interferometer that uses two stationary reflective diffraction gratings. Operation of the SHRS has been described previously.^{21–23} Briefly, collimated signal enters the input aperture of the SHRS where it is split into two beams by a 50:50 beamsplitter. These two beams strike the stationary diffraction gratings which are tilted at an angle, θ_L , such that one particular wavelength, the Littrow wavelength, λ_L , is retroreflected along the incident light path and recombines at the beamsplitter. Heterodyning in the interferometer occurs at the Littrow wavelength, so light at wavelengths longer or shorter than λ_L are diffracted from the gratings at an angle to the optical axis, resulting in crossed wavefronts, inducing a spatial phase shift, and generating a wavelength dependent, vertical interference pattern on the array detector. The intensity of the pattern is a function of position x on the detector, given by Eq. I

$$I(x) = \int_0^\infty B(\sigma) \{ 1 + \cos[8\pi(\sigma - \sigma_L)x \tan\theta_L] \} d\sigma \qquad (1)$$

where $B(\sigma)$ is the input spectral intensity at wavenumber σ , and the Fourier transform (FT) of I(x) recovers the encoded Raman spectrum. The fringe frequency on the detector is given by Eq. 2, where f is in fringes/cm, σ_L is the Littrow wavenumber, and σ is the wavenumber of interest. ²³

$$f = 4(\sigma - \sigma_L) \tan \theta_L \tag{2}$$

According to Eq. 2, emission lines above or below the Littrow wavelength show identical fringe patterns, leading to degenerate lines (i.e., line overlap). This degeneracy can be removed by tilting one of the gratings vertically or rotating it about the optical axis, which induces a rotation to the Fizeau fringe pattern, in opposite directions above and below Littrow. ^{22,23} In this case, a 2D Fourier transform can be used to recover spectra above and below the Littrow wavelength, unambiguously. This is very useful for doubling the spectral range of the SHRS.

Unlike a dispersive spectrometer, which requires a physical slit to control the spectral resolution, the SHRS, like other Fourier transform interferometers, does not. Rather, the resolving power, R, of the SHRS, given by Eq. 3 is equal to the total number of grooves illuminated on both gratings where W is the illuminated width of one grating and D is the grating line density.²³

$$R = 2WD \tag{3}$$

This allows the SHRS to employ a large entrance aperture, greatly increasing the throughput of the system, which is advantageous for measuring extended sources in situations where a large laser spot might be used to reduce sample damage; when using a large diameter optical fiber to deliver light to the spectrometer; or other applications where large sample areas need to be measured, such as the imaging technique described in this paper.

In the SHRS used for these studies (see Fig. 1a), the width of the input beam at the gratings is $\sim\!14\,\text{mm}$, so the theoretical resolving power, R, is 8400, giving a theoretical resolution of $\sim\!2\,\text{cm}^{-1}$ for a $1000\,\text{cm}^{-1}$ Raman band, using 532 nm excitation. This spectral resolution is about the same as a Kaiser Holospec f/1.8 spectrometer, with a 25 μm slit. The measured spectral resolution of the SHRS was $\sim\!7\,\text{cm}^{-1}$, using a low-pressure Hg lamp source (Ocean Optics, Hg-1). The measured resolution of the SHRS is very sensitive to alignment of focusing optics, likely the cause for the lower the expected resolution.

The illuminated width of the CCD is 14.8 mm, \sim 1100 pixels, so the theoretical spectral range of the SHRS, based on the Nyguist criteria of two pixels per wavelength, is \sim 1155 cm $^{-1}$. The spectral range can be doubled to \sim 2310 cm $^{-1}$ using the 2D Fourier transform technique described above. The throughput of the SHS is larger than a conventional dispersive spectrometer of comparable

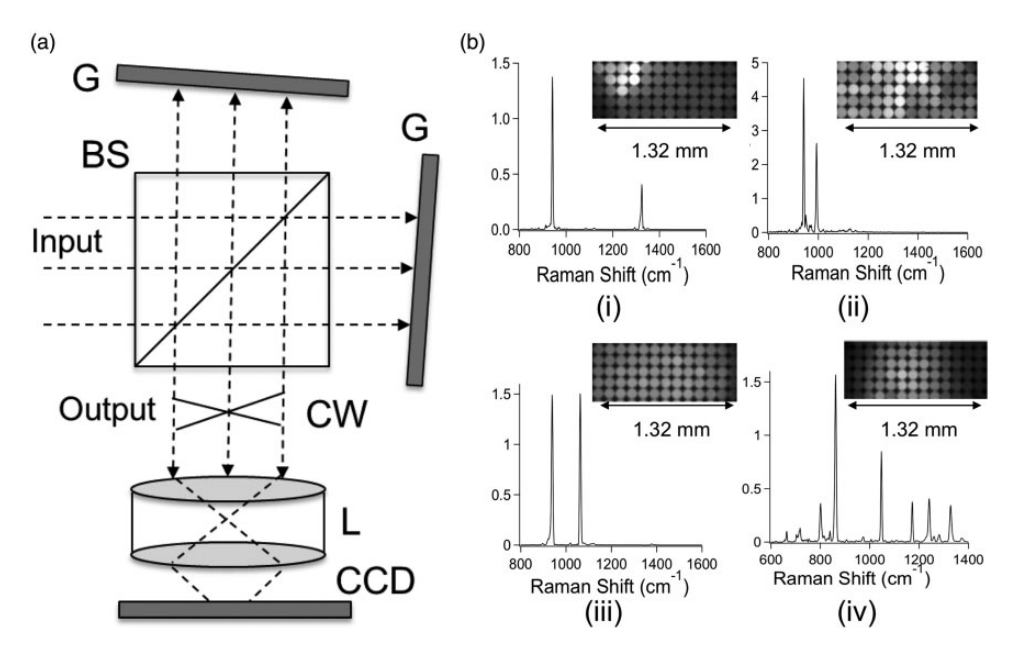


Figure I. (a) Spatial heterodyne spectrometer (SHS). BS: beam splitter; G: diffraction grating; CW: crossing wavefronts; L: lens; CCD: charge-coupled device detector. (b) Raman spectra measured by a SHS spectrometer for (i) a diamond in potassium perchlorate pellet, (ii) a sodium sulfate/potassium perchlorate bilayer pellet, (iii) a sodium nitrate/potassium perchlorate bilayer pellet, and (iv) an acetaminophen/ammonium nitrate bilayer pellet. Spectra shown are the result of Fourier transforming all lenslets on the CCD. One-lenslet spectra for samples (i)–(iii) are shown in Figs. 5 to 7; 150 mW CW 532 nm, (i) and (ii) 10 min acquisition, (iii) and (iv) 3 min acquisition.

spectral resolution, from the combination of a large aperture and wide FOV. The maximum, resolution-limited solid angle FOV of the SHRS is related to the resolving power by Eq. 4. 23 The solid angle FOV for the spectrometer used in the studies presented here is $7.5\times10^{-4}\,\mathrm{sr}$, corresponding to a full acceptance angle of $\sim\!1.6^\circ$

$$\Omega_{\text{max}} = 2\pi/R \tag{4}$$

Figure 2a shows how the MLA is imaged onto the face of the gratings by the relay lens. The 40×40 MLA used in this work is shown in Fig. 2b. Light from each MLA lenslet travels in a unique path through the interferometer, each providing its own independent spatially isolated Fizeau fringe pattern. In Fig. 2a, the light path for two lenslets is illustrated. Each of the 1600 MLA lenslets (Fig. 2b) has the same focal length, and the sample is placed one focal length from the MLA. The laser is focused by each MLA lenslet to a small spot on the sample. Scattered Raman light is collected by the MLA lenslets to produce an array of collimated beams, one for each lenslet. As long as the beams generated by the f/16 MLA lenslets are collimated within the acceptance angle of the SHRS, interference occurs producing high contrast fringe patterns. The relay lens is positioned to image the back surface of the MLA onto the SHRS gratings. A spatial filter, located at the focal point of the relay lens, prevents crosstalk between the FOV of MLA lenslets, as described by Tiziani et al. 19,20 Another lens inside the SHRS images the grating face, i.e., the focused

MLA lenslet image, onto a CCD detector. Figure 2c is the Raman image of the sulfur pellet in Fig. 2d, which shows almost all of the 1600 MLA lenslets and the ridge detail of the sulfur pellet that is retained in the MLA-SHRS image. However, with the CCD used for this work, individual lenslet Fizeau fringes could not be resolved. This is a limitation of the number of pixels in our detector array, which, at only eight pixels per lenslet, was insufficient to resolve fringes. Resolving all 1600 lenslet fringe images would require a CCD with much smaller pixels.

Figure 1b shows Raman spectra measured using the MLA-SHRS system shown in Fig. 2. Each detector image with its corresponding spectrum shows the individual lenslets that are viewed and the position of each sample within the FOV. The samples consisted of a series of bilayer pellets that were illuminated at the interface between the two constituents, so that both solids were within the FOV of the instrument. The imaged area shown was about 12 lenslets wide by about five lenslets tall, giving a measured sample area of 1.32 mm \times 0.55 mm. The number of lenslets viewed was limited by the spectral resolution of the grating used in these studies-these limitations are discussed in a later section. For the spectra shown, the MLA was not used for imaging, rather, the signal from all 60 lenslets was summed to produce the spectrum, which represents the mean Raman spectra over the total area measured. The measured resolution was $\sim 7 \, \mathrm{cm}^{-1}$ for the potassium perchlorate/diamond and sodium sulfate/potassium perchlorate samples. The resolution was slightly lower, \sim 8–9 cm⁻¹,

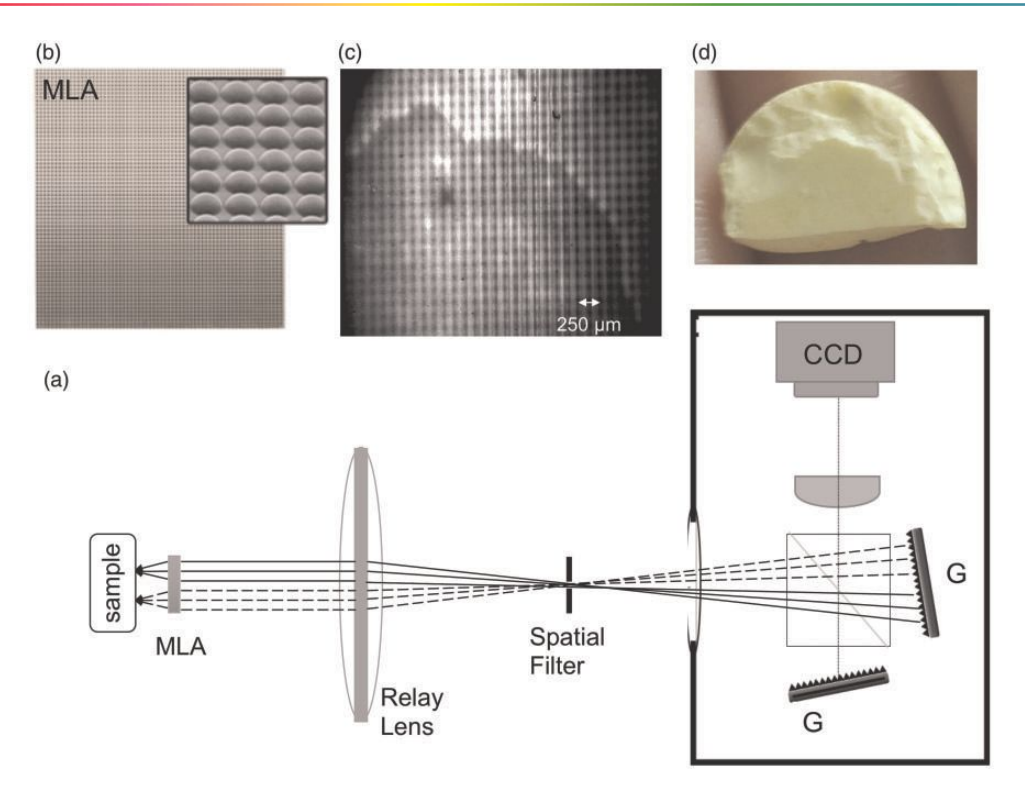


Figure 2. (a) Schematic of the optical path of the MLA-SHRS. G: diffraction grating; CCD: charge-coupled device detector. (b) A microlens array illustration. A Raman image (c) for a sulfur pellet (d) measured with the MLA-SHRS showing almost all 1600 MLA lenslets being used.

for the sodium nitrate/potassium perchlorate and an acetaminophen/ammonium nitrate pellets, because the imaging magnification was slightly larger (8×) than in the former (10×). The spectral range for these spectra is $\sim\!1150\,\mbox{cm}^{-1}$, consistent with the theoretical value. Raman spectra using fringe images from the individual lenslets, for each of the samples shown in Fig. 1b, are described in the following.

Figure 3 shows how MLA-SHRS lenslet spectra are recovered for a diamond sample. The signal is collected and shown as an array of fringe images (upper left image), one from each lenslet, on the detector. The fringe image cross-section (upper right), produced by summing pixels vertically in each column, for a selected lenslet fringe image (shown by white box), shows an interferogram superimposed on a large background signal. The background is removed by subtracting a fitted polynomial from the cross-section. This subtraction procedure does not account for the variation of the signal intensity across the interferogram. The spectrum is obtained by taking the one-dimensional (ID) Fourier transform of the resulting interferogram. The resulting diamond Raman spectrum has a spectral resolution of ~41 cm⁻¹, which is lower than the 6 cm⁻¹ achieved for the diamond sample shown in Fig. 1b(i), because of the lower number of grooves illuminated by a single lenslet on the grating. Due to coherence effects inside the interferometer, each MLA lenslet interferogram does not have its own location of zero path difference. This results in a decrease of coherence across the grating face and limits the horizontal size of the grating that can give high fringe contrast across the entire grating face. A solution to this issue would be to use several smaller gratings, each with its own center burst position, or use a compensator plate, shaped to reduce the optical path difference across the grating.

A 2D Fourier transform of each lenslet Fizeau fringe pattern can be used to differentiate spectra on either side of the Littrow (i.e., the heterodyne) wavelength and approximately double the spectral range, provided the fringe pattern has a sufficient rotation to induce a phase shift, ϕ , along the *y*-axis. This is accomplished by either tilting or rotating one of the gratings with respect to the other grating in the SHRS. An expansion of the bracketed term in Eq. I to include this *y*-axis phase shift term is shown in Eq. 5 23

$$I(x,y) = \int_0^\infty B(\sigma) \{ 1 + \cos[2\pi(4(\sigma - \sigma_L)x \tan\theta_L + y\sigma\varphi)] \} d\sigma$$
(5)

Figure 4 shows a 2D interferogram for an acetaminophen sample (top left), cropped to show clearly the crossed

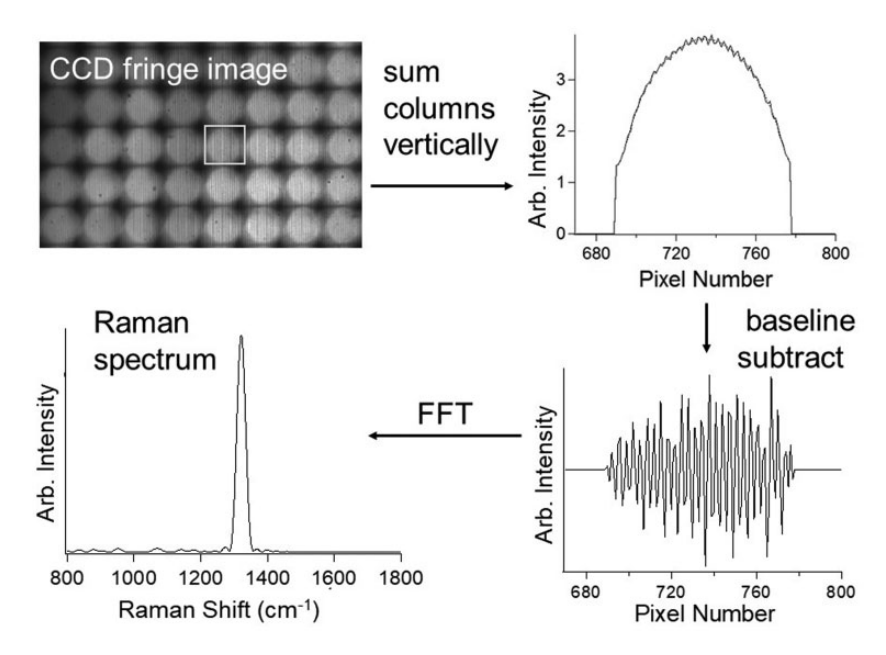


Figure 3. How to recover one-lenslet spectra using the MLA-SHRS. The signal is collected and measured as a fringe image on the detector (upper left). The one lenslet region of interest, shown in white, is chosen and the columns are summed to provide an interferogram superimposed on a background signal (upper right). The interferogram (lower right) is obtained by subtracting a polynomial fit, and the spectrum (lower left) is obtained by taking the one-dimensional Fourier transform of the interferogram. The sample for the spectrum shown is diamond.

fringe pattern, for a 4×4 section of lenslets. The Littrow wavenumber of the SHRS was set to \sim 1000 cm $^{-1}$, indicated by σ_l in the spectra, so Raman bands above and below Littrow rotate the fringes in opposite directions. Note the strong center burst in region b of the Raman fringe image. Raman spectra (right) for the regions a-c, labeled on the detector fringe image were obtained using a 2D Fourier transform. The spectrum labeled d is a reference Raman spectrum of acetaminophen from the RRUFF database (RRUFF ID D120007).25 Using the MLA-SHRS for Raman imaging, there is a tradeoff between spectral resolution and number of lenslets used in the horizontal direction (e.g., grating grooves illuminated). For example, the spectra produced by region a for a single lenslet, and region b which covers four lenslets vertically, produce spectra with the same resolution, \sim 42 cm⁻¹, because both regions illuminate the same number of grating grooves. However, the spectrum produced by region c, viewing four lenslets horizontally, has four times higher resolution, \sim 11 cm $^{-1}$, because four times as many grating grooves were illuminated. The intensity scales with the number of lenslets viewed, regardless of the direction.

Figure 5 shows the Raman image (top left) for a diamond/perchlorate sample (top right). In this image, the MLA was magnified by $10\times$ onto the gratings, and 60 different lenslets are shown, corresponding to a sampled area on the sample of $1.32\times0.55\,\mathrm{mm}^2$. Lenslets outside this area did not show high contrast fringes. The image is brighter in the diamond region because the diamond

Raman cross-section is $\sim\!\!3.8$ times larger than perchlorate. ^{26,27} Spectra corresponding to three different sample regions are shown (bottom left). Region a shows only the diamond Raman band at 1332 cm $^{-1}$, region b shows both potassium perchlorate and diamond Raman bands, and region c shows only the 941 cm $^{-1}$ Raman band of potassium perchlorate. ^28.29

The size of the image of each lenslet on the gratings is 0.98 mm. For the 300 lp/mm gratings, this corresponds to a theoretical resolving power of 588, which gives a theoretical spectral resolution of $32\,\mathrm{cm}^{-1}$. The measured resolution of the spectra shown in Fig. 5 are consistent with this value, at $33\,\mathrm{cm}^{-1}$. The grating image is magnified 1.17× on the CCD, so each lenslet has a diameter of 85 pixels, thus allowing 85/2 spectral elements to be measured, giving a theoretical spectral range of 1360 cm $^{-1}$. The observed one-lenslet spectral range, $\sim 1250\,\mathrm{cm}^{-1}$, is consistent with this value.

The Raman image in Fig. 6 (top left), measured in the same configuration as in Fig. 5, shows an example of resolving close lying Raman bands for two samples, sodium sulfate/potassium chlorate, that are separated by no more than two lenslet diameters. The interface between the samples, labeled in the picture inset with a dashed line, is not immediately obvious in the white light image, because both constituents have similar Raman scattering cross-sections. The measured spectral resolution for the Raman spectra (bottom left) of the three lenslet regions (a, b, and c) is $\sim\!33\,\mathrm{cm}^{-1}$, adequate to distinguish between the sodium

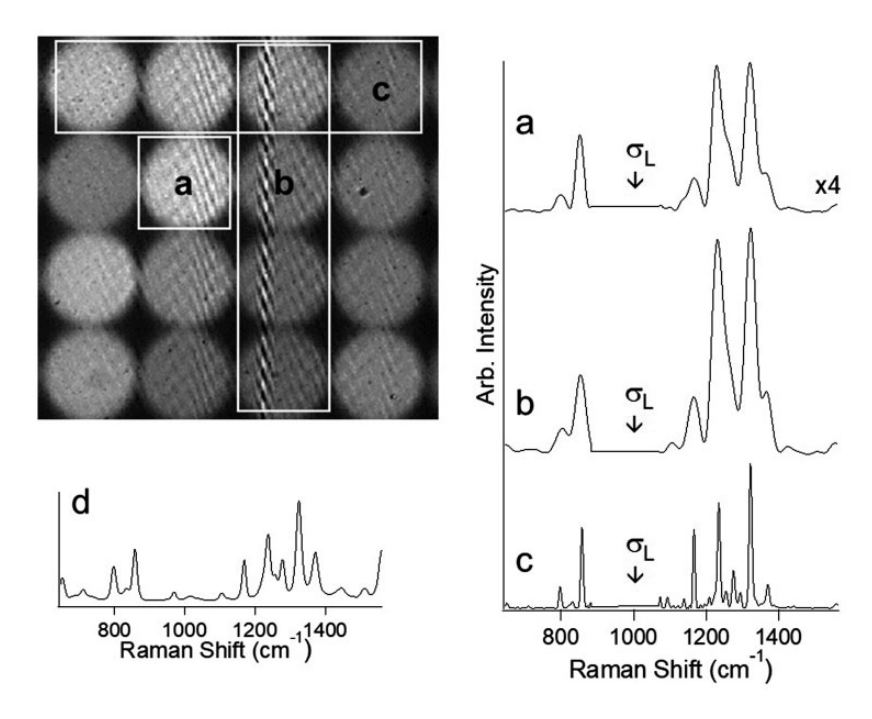


Figure 4. Left: The Raman image of an acetaminophen pellet measured using our MLA-SHRS in 2D-SHS configuration. The interferogram image is labeled with (a) a one lenslet region of interest, (b) a column of four lenslets, and (c) a row of four lenslets. Right: the spectra for each region of interest are shown. Littrow wavenumber is around $1000 \, \mathrm{cm}^{-1}$, as indicated by σ_L . Spectrum (d) is an acetaminophen reference Raman spectrum provided via RRUFF database (RRUFF ID: D120007).

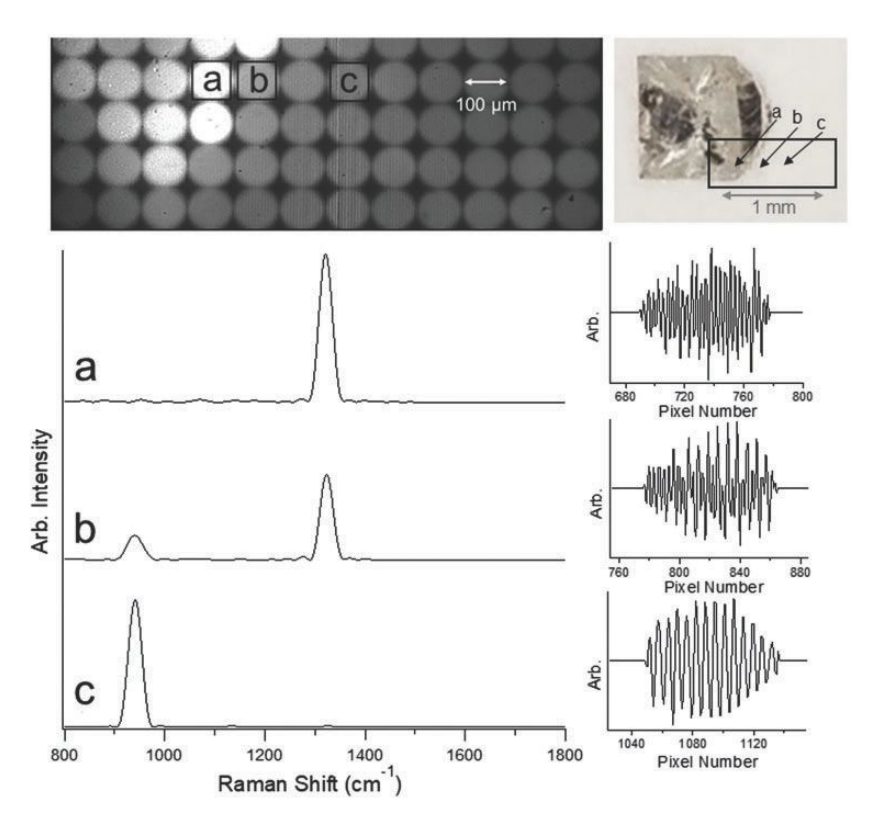


Figure 5. Diamond in perchlorate measured with the MLA-SHRS in 1D SHRS configuration. Top left: the Raman image labeled with the one-lenslet regions of interest. Top right: picture of the sample with black box labeling the area measured. Bottom left: spectra corresponding to each one lenslet region of interest, offset for clarity. Bottom right: the corrected interferograms for each region of interest.

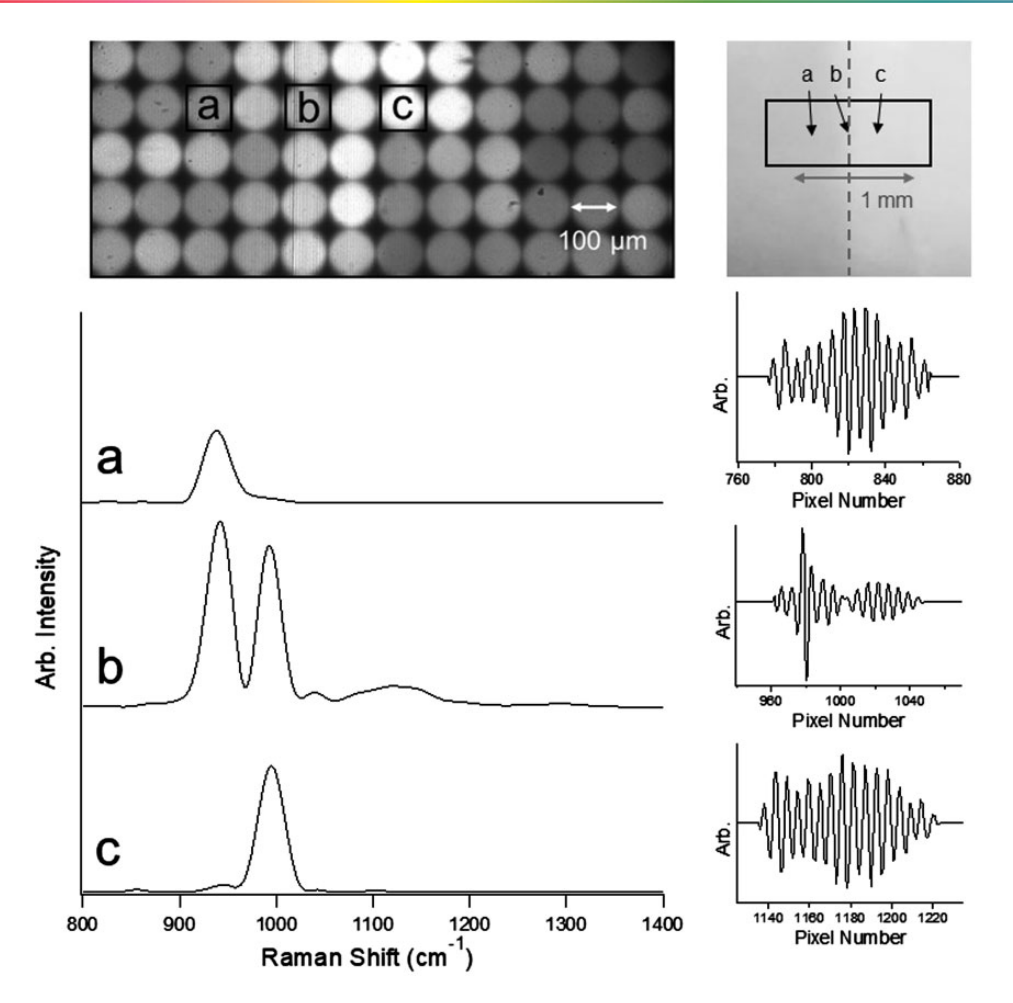


Figure 6. A sodium sulfate/potassium chlorate bilayer pellet measured with the MLA-SHRS in 1D SHRS configuration. Top left: the Raman image labeled with the one-lenslet regions of interest. Top right: picture of the sample with black box indicating the area measured and gray dashed line to indicate the interface on the sample. Bottom left: spectra corresponding to each one lenslet region of interest, offset for clarity. Bottom right: the corrected interferograms for each region of interest.

sulfate band at 990 cm⁻¹ and potassium perchlorate Raman band at 941 cm⁻¹. Note, in this case, the brightness of the lenslets in the Raman image is not indicative of the sample type because in these images we did not correct for changes in light intensity across the image, as might occur from such things as changes in laser power, sample position or flatness with respect to the MLA image plane, density variations in the sample, sample refractive index differences, or luminescence impurities in the samples.

For transparent, highly scattering samples, the spatial resolution of any Raman imaging technique is limited by diffuse scattering of the laser through the sample, so the laser is not localized at the focal point of the laser but can excite Raman scattering up to many millimeters away. Spatially offset Raman takes advantage of this effect, to increase the volume that is probed for highly scattering samples such as pharmaceutical tablets. ¹⁵ This is illustrated by the Raman image in Fig. 7, for a sodium nitrate/potassium perchlorate sample (top right). In this image, Raman from 60 different MLA lenslets is shown, covering an area

on the sample of about 1.32×0.55 mm, the magnification was $8 \times$ on the gratings. Normalized Raman spectra from eight selected lenslet regions are shown (left). The resolving power per lenslet is 450, which corresponds to a spectral resolution of $41.7 \, \mathrm{cm}^{-1}$, which matches the measured resolution of $42 \, \mathrm{cm}^{-1}$. The grating image is magnified $1.17 \times$ on the CCD, so each lenslet image has a diameter of 65 pixels, thus allowing 65/2 spectral elements to be measured, giving a theoretical spectral range of $1365 \, \mathrm{cm}^{-1}$. The observed one-lenslet spectral range, $\sim 1250 \, \mathrm{cm}^{-1}$, is consistent with this value.

If there were no overlap between the Raman signals collected by the lenslets of the array for the bilayer sample used here, we would expect the Raman spectra to change rapidly for lenslets on either side of the sample interface, showing only nitrate (1062 cm⁻¹) on one side and only perchlorate (941 cm⁻¹) on the other side.³⁰ So, a plot of the intensity ratio of these two bands would show an abrupt change at the interface. Instead, what we see is a more gradual intensity ratio change, due to diffuse

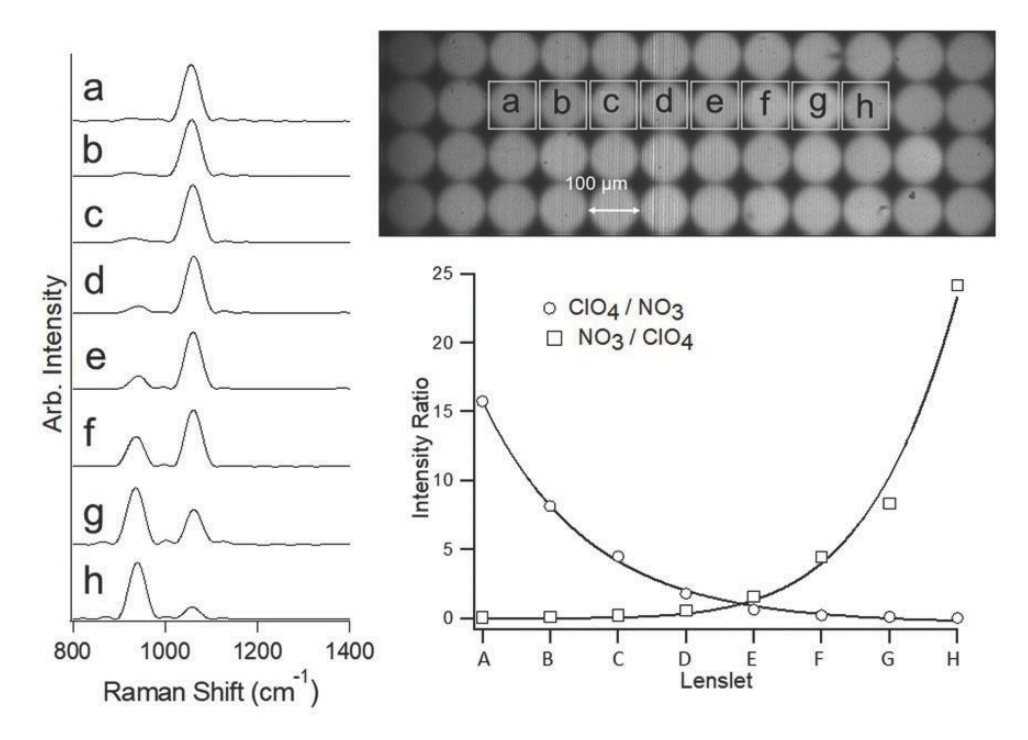


Figure 7. A sodium nitrate/potassium perchlorate bilayer pellet measured with the MLA-SHRS in ID SHRS configuration. Top right: the Raman image labeled with one-lenslet regions of interest. Left: normalized spectra corresponding to each one-lenslet region of interest, offset for clarity. Bottom right: Intensity ratios of the KClO₄ and NaNO₃ bands plotted versus lenslet location.

scattering in the sample, as shown in Fig. 7 (lower right). The intensity ratio is shown in this plot, because the Raman intensity changes a lot from lenslet to lenslet and this was not corrected. The shape of the intensity ratio curves in Fig. 7 is consistent with plots of Raman signal intensity versus relative offset position for spatially offset Raman. In fact, the MLA-SHRS hyperspectral imaging system described here would seem to be ideal for quickly making measurements that can be used to test models of spatially offset and transmission Raman.

Figure 8 shows a Raman image made up of 546 lenslets (top left) for a diamond/potassium perchlorate sample, with each lenslet showing clear interference fringes. To acquire this image, the MLA was magnified by $4\times$ onto the 150 lp/ mm gratings. The 546 lenslets shown correspond to an area on the sample of $2.31 \times 2.86 \, \text{mm}^2$. A CMOS detector (AgenaAstroproducts, QHY183M) with 2.4 µm pixels and overall chip size of $13 \times 8 \, \text{mm}^2$ was used to acquire this image. The cross-section (bottom) for a selected row of lenslets shows high contrast fringes for each lenslet. Raman spectra, recovered by taking the Fourier transform of the cross-section for two individual lenslets are shown (top right), for lenslets that image diamond and perchlorate regions of the sample. The size of the image of each lenslet on the gratings is 0.4 mm. For the 150 lp/mm gratings, this corresponds to a theoretical resolving power of 120, which gives a theoretical spectral resolution of 148 cm⁻¹. The measured resolution of the spectra shown in Fig. 8 is consistent with this value, at 148 cm⁻¹. This low spectral resolution is limited by the grating groove density and the total number of pixels available on the detector.

Imaging Limitations of the MLA-SHRS

For the MLA-SHRS technique, the number of spatial elements that can be imaged simultaneously is determined by the grating size and the desired spectral resolution, and also depends on the laser wavelength. For an individual lenslet, the resolution is determined primarily by the number of grating grooves that are illuminated by that lenslet. Table I shows the theoretical maximum number of spatial elements that can be imaged using a 25 mm SHRS, for three different laser wavelengths and grating groove densities, assuming a spectral resolution of 20 cm⁻¹. The calculations show that using 785 nm or 532 nm laser wavelength, over 10 000 spatial points can be simultaneously imaged, with a spectral range that is limited only by the number of pixels available on the detector. Even at 244 nm, almost 4000 lenslets can theoretically be measured. Furthermore, if 30 cm⁻¹ spectral resolution is permissible, then \sim 23 000 lenslets could be imaged at the longer wavelengths. These calculations do not account for loss of coherence across the SHRS grating face. Because the initial SHRS alignment was performed along the center of the optical axis, the loss of coherence will limit the contribution of lenslets far from the center of the grating in the horizontal direction (i.e., parallel to the

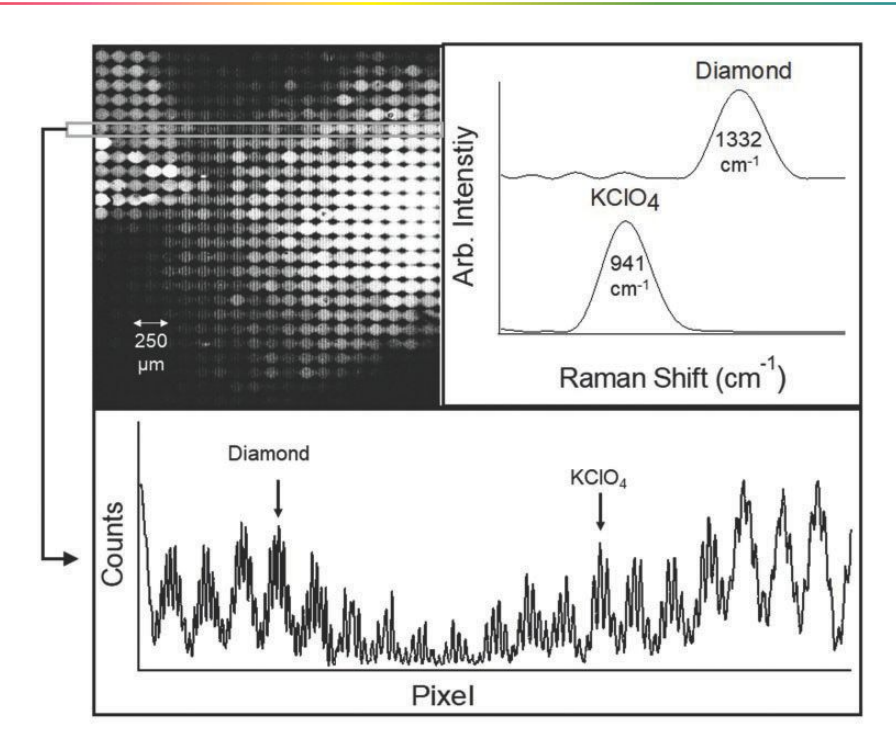


Figure 8. Top left: the Raman image of diamond in perchlorate, measured with MLA magnified $4\times$ onto the SHRS gratings in 1D SHRS configuration. Bottom: the cross-section for the row of lenslets outlined in gray on the Raman image. Top right: Raman spectra corresponding to two different lenslets.

Table I. The performance characteristics for an MLA-SHRS for system that has 20 cm⁻¹ resolution for one-lenslet spectra.

Wavelength (nm)	Grating line density (lp/mm)	Grooves illuminated per lenslet for 20 cm ⁻¹ spectral resolution	lmaged lenslet diameter (μm)	Number of lenslets, horizontal direction ^a	Total lenslets imaged
785	1200	293	244	103	10 609
532	1800	444	247	101	10201 ^b
244	2400	999	416	60	3600

^a25 mm grating width.

grating dispersion). The extent of this depends on the coherence length of the bands being measured and the grating Littrow angle. In situations where loss of coherence might occur, physically offset compound gratings, a curved grating, or possibly a refractive optic could be designed to mitigate the problem.

Conclusion

A new hyperspectral Raman imaging technique is demonstrated using an SHRS with an MLA, where the entire hypercube of spatial and spectral information is obtained in a single measurement. Raman images for a variety of sample types are demonstrated where Raman spectra, at spectral ranges from $1200\,\mathrm{cm}^{-1}$ to $2800\,\mathrm{cm}^{-1}$, were acquired for 60 to >500 unique spatial points dependent

on the type of detector used. The spectral resolution of the Raman spectra acquired for each spatial point in the images varied from 32 cm⁻¹ to 148 cm⁻¹, dependent on the grating and system magnification. Calculations show that this technique can be extended to include more than 10 000 spatial points with a spectral resolution of 20 cm⁻¹, with a large spectral range. Loss of coherence across the grating can be compensated using multiple gratings, each with its own center burst position, or using a compensator plate, shaped to reduce the optical path difference across the grating.

Declaration of Conflicting Interests

The author(s) declared no potential conflicts of interest with respect to the research, authorship, and/or publication of this article.

^b23 095 lenslets at 30 cm⁻¹ spectral resolution.

Funding

We would like to thank the National Science Foundation (grant numbers CHE-1308211 and OCE-1829333) and NASA (grant numbers NNX14Al34G and 80NSSC19K1024) for funding this work. This work was also performed, in part, under the auspices of the U.S. Department of Energy by Lawrence Livermore National Laboratory under Contract DE-ac52-07NA27344.

ORCID iDs

References

- J.M. Harlander, F.L. Roesler, C.R. Englert, et al. "Robust Monolithic Ultraviolet Interferometer for the SHIMMER Instrument on STPsat-I". Appl. Opt. 2003. 42(15): 2829–2834.
- S.M. Angel, T.J. Kulp, T.M. Vess. "Remote-Raman Spectroscopy at Intermediate Ranges Using Low-Power CW Lasers". Appl. Spectrosc. 1992. 46(7): 1085–1091.
- A. Allen, S.M. Angel. "Miniature Spatial Heterodyne Spectrometer for Remote Laser Induced Breakdown and Raman Spectroscopy Using Fresnel Collection Optics". Spectrochim. Acta, Part B. 2018. 149: 91–98.
- P.J. Treado, I.W. Levin, E.N. Lewis. "Near-Infrared Acousto-Optic Filtered Spectroscopic Microscopy: A Solid-State Approach to Chemical Imaging". Appl. Spectrosc. 1992. 46(4): 553–559.
- 5. M. Delhaye, P. Dhamelincourt. "Raman Microprobe and Microscope with Laser Excitation". J. Raman Spectrosc. 1975. 3(1): 33–43.
- C.J.H. Brenan, I.W. Hunter. "Chemical Imaging with a Confocal Scanning Fourier-Transform-Raman Microscope". Appl. Opt. 1994. 33(31): 7520–7528.
- M. Bowden, D.J. Gardner, G. Rice, et al. "Line-Scanned Micro Raman Spectroscopy Using a Cooled CCD Imaging Detector". J. Raman Spectrosc. 1990. 21(1): 37–41.
- 8. D.N. Batchelder, C. Cheng, G.D. Pitt. "Molecular Imaging by Raman Microscopy". J. Adv. Mater. 1991. 3(11): 566–568.
- G.J. Puppels, M. Grond, J. Greve. "Direct Imaging Raman Microscope Based on Tunable Wavelength Excitation and Narrow-Band Emission Detection". Appl. Spectrosc. 1993. 47(8): 1256–1267.
- PJ. Treado, I.W. Levin, E.N. Lewis. "High-Fidelity Raman Imaging Spectrometry: A Rapid Method Using an Acousto-Optic Tunable Filter". Appl. Spectrosc. 1992. 46(8): 1211–1216.
- H.T. Skinner, T.F. Cooney, S.K. Sharma, et al. "Remote Raman Microimaging Using an AOTF and a Spatially Coherent Microfiber Optical Probe". Appl. Spectrosc. 1996. 50(8): 1007–1014.
- H.R. Morris, C.C. Hoyt, P. Miller, et al. "Liquid Crystal Tunable Filter Raman Chemical Imaging". Appl. Spectrosc. 1996. 50(6): 805–811.

- S. Saeed, P.J. Bos. "Multispectrum, Spatially Addressable Polarization Interference Filter". J. Opt. Soc. Am. A. 2002. 19(11): 2301–2312.
- J.W. Evans. "The Birefringent Filter". J. Opt. Soc. Am. 1949. 39(3): 229–242.
- S. Stewart, R.J. Priore, M.P. Nelson, et al. "Raman Imaging". Annu. Rev. Anal. Chem. 2012. 5: 337–360.
- K.A. Christensen, N.L. Bradley, M.D. Morris, et al. "Raman Imaging Using a Tunable Dual-Stage Liquid Crystal Fabry–Perot Interferometer". Appl. Spectrosc. 1995. 49(8): 1120–1125.
- J. Ma, D. Ben-Amotz. "Rapid Micro-Raman Imaging Using Fiber-Bundle Image Compression". Appl Spectrosc. 1997. 51(12): 1845–1848.
- J.G. Dwight, T.S. Tkaczyk. "Lenslet Array Tunable Snapshot Imaging Spectrometer (LATIS) for Hyperspectral Fluorescence Microscopy". Biomed. Opt. Express. 2017. 8(3): 1950–1964.
- H.J. Tiziani, H.M. Uhde. "Three-Dimensional Analysis by a Microlens-Array Confocal Arrangement". Appl. Opt. 1994. 33(4): 567–572.
- H.J. Tiziani, R. Achi, R.N. Kramer, L. Wiegers. "Theoretical Analysis of Confocal Microscopy with Microlenses". Appl. Opt. 1996. 35(1): 120–125.
- N.R. Gomer, C.M. Gordon, P. Lucey, S.K. Sharma, et al. "Raman Spectroscopy Using a Spatial Heterodyne Spectrometer: Proof of Concept". Appl. Spectrosc. 2011. 65(8): 849–857.
- N. Lamsal, S.K. Sharma, T.E. Acosta, S.M. Angel. "Ultraviolet Stand-Off Raman Measurements Using a Gated Spatial Heterodyne Raman Spectrometer". Appl. Spectrosc. 2016. 70(4): 666–675.
- J.M. Harlander. Spatial Heterodyne Spectroscopy: Interferometric Performance at Any Wavelength Without Scanning. [Doctoral Dissertation]. Madison, Wisconsin: The University of Wisconsin, 1991.
- Kasier Optical Systems, Inc. Holospec Imaging Spectrograph Operations Manual. v.2.0. 2002. https://psfcsv10.psfc.mit.edu/ ~rowan/page4/page6/assets/holospec_v2.pdf [accessed Oct 31 2019].
- B. Lafuente, R.T. Downs, H. Yang, et al. "The Power of Databases: The RRUFF Project". In: T. Armbruster, R.M. Danisi, W. de Gruyter, editors. Highlights in Mineralogical Crystallography. Berlin: Walter de Gruyter GmbH, 2015. Pp. 1–30.
- R.L. Aggarwal, L.W. Farrar, S.K. Saikin, et al. "Measurement of the Absolute Raman Cross Section of the Optical Phonons in Type la Natural Diamond". Solid State Commun. 2012. 152: 204–209.
- T.E. Acosta-Maeda, A.K. Misra, J.N. Porter, et al. "Remote Raman Efficiencies and Cross-Sections of Organic and Inorganic Chemicals". Appl. Spectrosc. 2017. 71(5): 1025–1038.
- S.A. Solin, A.K. Ramdas. "Raman Spectrum of Diamond". Phys. Rev. B. 1970. 1(4): 1687–1698.
- N. Krishnamurthy. "Raman Spectrum of Crystalline Potassium Perchlorate". Proc. Ind. Acad. Sci., A. 1965. LXI: 118–121.
- D.L. Rousseau, R.E. Miller. "Raman Spectrum of Crystalline Sodium Nitrate". J. Chem. Phys. 1968. 48(8): 3409–3413.
- P. Matousek, I.P. Clark, E.R.C. Draper, et al. "Subsurface Probing in Diffusely Scattering Media Using Spatially Offset Raman Spectroscopy". Appl. Spectrosc. 2005. 59(4): 393–400.